Nonlinear Plasmonic Nanorulers

Jérémy Butet* **and Olivier J. F. Martin**

Nanophotonics and Metrology Laboratory (NAM), Swiss Federal Institute of Technology Lausanne (EPFL), 1015, Lausanne, Switzerland

ABSTRACT The evaluation of distances as small as few nanometers using optical waves is a very challenging task that can pave the way for the development of new applications in biotechnology and nanotechnology. In this article, we propose a new measurement method based on the control of the nonlinear optical response of plasmonic nanostructures by means of Fano resonances. It is shown that Fano resonances resulting from the coupling between a bright mode and a dark mode at the fundamental wavelength enable unprecedented and direct manipulation of the nonlinear electromagnetic sources at the nanoscale. In the case of second harmonic generation from gold nanodolmens, the different nonlinear sources distributions induced by the different coupling regimes are clearly revealed in the far-field distribution. Hence, the configuration of the nanostructure can be accurately determined in 3-dimensions by recording the wave scattered at the second harmonic wavelength. Indeed, the conformation of the different elements building the system is encoded in the nonlinear far-field distribution, making second harmonic generation a promising tool for reading 3-dimension plasmonic nanorulers. Furthemore, it is shown that 3-dimension plasmonic nanorulers can be implemented with simpler geometries than in the linear regime while providing complete information on the structure conformation, including the top nanobar position and orientation.

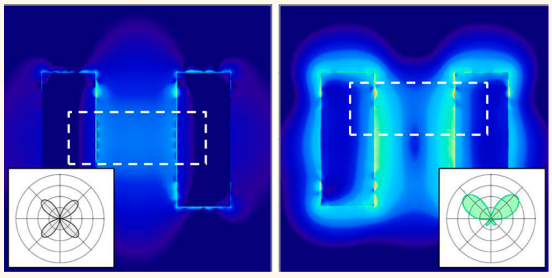

KEYWORDS: plasmon · nonlinear optics · nanoruler · second harmonic generation · fano resonances · optical antenna

Plasmonic nanostructures play an important role in the development of applications in nanophotonics.[1] These nanostructures have unique and interesting optical properties thanks to surface plasmon resonances, which correspond to the collective oscillations of the conduction electrons.[2] These resonances are associated with a strong scattering and absorption, as well as localization of light far below the diffraction limit.[3,4] The coupling and hybridization between plasmon modes is a common technique for tailoring and controlling their optical properties.[5,6] The interaction between plasmon modes changes significantly with the distance between their supporting structures, allowing the design of plasmonic nanorulers, the optical responses of which vary with the conformation of the different nanoelements that compose them.[7,8] These plasmonic rulers were found to be very useful for the observation of biological and chemical processes down to the nanoscale.[9−12] Recently, significant attention was paid to plasmonic nanostructures supporting Fano resonances.[13,14] As examples, Fano resonances have been reported in ring-disk nanocavities,[15−17] dolmens[18−20] and plasmonic oligomers.[21−24] Several theoretical models were developed to describe Fano resonances and their characteristic asymmetric line shape in terms of coupling between optical dark and bright modes.[25−28] It was also shown that Fano resonances can also arise from the coupling between bright modes only.[29] In specific plasmonic Fano systems, the interaction between bright and dark modes leads to a window of transparency similar to the electromagnetically induced transparency observed in atomic physics.[30,31] Because of their narrower spectral width compared to conventional plasmon resonances and larger induced field enhancement, Fano resonances have been used for a variety of applications including plasmonic rulers[32,33] and biosensors.[17,34−36] The optical response of nanosystems close to a metallic surface strongly depends on the distance between this object and the surface allowing measurement of very small separations with high sensitivity.[37,38] Recently, 3-dimensional plasmonic rulers based on Fano resonances were designed in the perspective of the determination of the complete spatial configuration of complex macromolecular entities as well as their dynamic evolution.[39] Nevertheless, the fabrication of these 3-dimensional complex plasmonic rulers is very challenging, and disposing of a way of

* Address correspondence to jeremy.butet@epfl.ch.

Received for review February 17, 2014 and accepted April 3, 2014.

Published online April 03, 2014
10.1021/nn500943t

determining nanoscale distances in 3-dimensions using a simpler ruler structure would open up new application possibilities. Here we show that a nonlinear readout for a simple ruler geometry can provide such configuration information in 3-dimensions.

Over the past decade, a significant effort has been devoted to the study of the nonlinear optical properties of plasmonic nanostructures.[40] Among the different nonlinear optical processes, second harmonic generation (SHG), whereby two photons at the fundamental frequency are converted into one at the second harmonic (SH) frequency, is the simplest and the most studied.[41−48] The polarization and shape dependence of the SH intensity has been investigated for both centrosymmetric and noncentrosymmetric metallic nanostructures.[41−48] Several studies have reported the observation of SHG from single metallic nanostructures, paving the way for the design of practical applications as nonlinear plasmonic sensing,[49] sensitive shape characterization[50,51] and imaging,[52−54] as well as detailed determination of the surface plasmon resonance properties.[55−57] For practical applications, it is also important to increase the nonlinear conversion at the nanoscale and multiresonant plasmonic nanostructures were found to be an efficient method to do so.[58−60] However, the use of Fano resonances in nonlinear plasmonics has barely been studied, compared to the linear case.[61−63]

In this article, the SHG from gold nanodolmens supporting Fano resonances is numerically investigated using a surface integral equations method. The influence of the structure asymmetry on the fundamental and SH near-field intensity distributions is discussed in detail. The SH waves induced by the nonlinear sources supported by the top bar, and the two parallel nanorods interfere in the far-field leading to specific SH emission patterns. The influence of the top nanorod position is systemically investigated, demonstrating that its position can be accurately determined in 3-dimensions by recording the SH wave scattered in the far-field. These results demonstrate that SHG is promising for reading the complete configuration of plasmonic rulers, allowing simpler geometries than in the linear regime to be used.

RESULTS AND DISCUSSION

The nonlinear plasmonic ruler discussed in this article is shown in Figure 1, where the different geometrical parameters are introduced. The considered nanostructure is composed of three nanorods: A gold nanorod is placed on top of two parallel gold nanorods. The three nanorods are 100 nm long, and their width w is 40 nm. The separation between the two parallel nanorods d is 60 nm. This gold nanodolmen is excited by an incident plane wave polarized along the x-axis and propagating along the z-axis. The top nanorod supports a dipolar plasmonic mode which can strongly

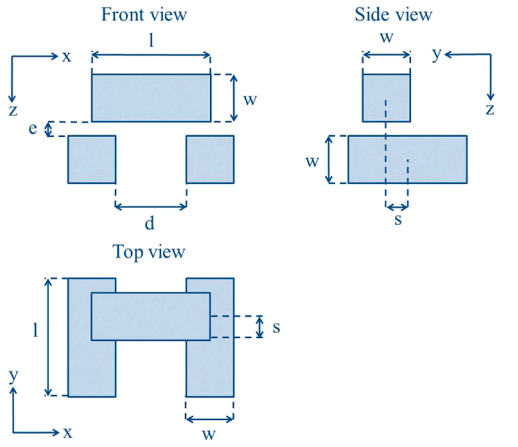

Figure 1. Schematic of the dolmen nanostructures studied in this work and definition of the geometrical parameters: $l = 100$ nm, $d = 60$ nm, and $w = 40$ nm. The parameters s and e are modified, and their values are specified throughout the manuscript.

couple to an incoming plane wave and can efficiently radiate light. On the contrary, the two bottom parallel nanorods support a quadrupolar plasmonic mode arising from plasmonic hybridization.[5] The out of phase dipole moments supported by each parallel nanorod prevent this quadrupolar mode from efficiently radiating light in the far-field. As a consequence, the quadrupolar mode cannot be excited by the homogeneous field of an incoming plane wave. The backward scattered intensity is evaluated using a surface integral equation method[64,65] as a function of the incident wavelength for different values of the symmetry breaking parameter s (Figure 2(a)) (see the Methods section for details). In the symmetric case, corresponding to $s = 0$ and the top bar situated at the center of the two parallel nanorods, a strong enhancement of the backward scattered intensity is observed at 780 nm, corresponding to the resonant excitation of the dipolar mode supported by the top nanorod.[33] Indeed, the coupling between the dipolar and the quadrupolar modes vanishes in the symmetric case and only the dipolar mode is excited by an incoming plane wave (see Figure 2(b,d)). As the asymmetry of the nanostructure increases, the optical response of the dolmen nanostructure dramatically evolves from a strong resonance to an antiresonance (dip).[31,33] For intermediate values of the symmetry parameter s, asymmetric spectral responses are observed as a consequence of the coupling between the dipolar and the quadrupolar modes. Even though the quadrupolar mode is not coupled to far-field radiation, this mode can be excited through its coupling with the dipolar mode, thanks to the Fano resonance (see Figure 2(e)).[33,36,66] In the following, we will show that a change in the near-field intensity distribution induced by excitation of the quadrupolar mode dramatically modifies the nonlinear optical response of the gold nanodolmen,

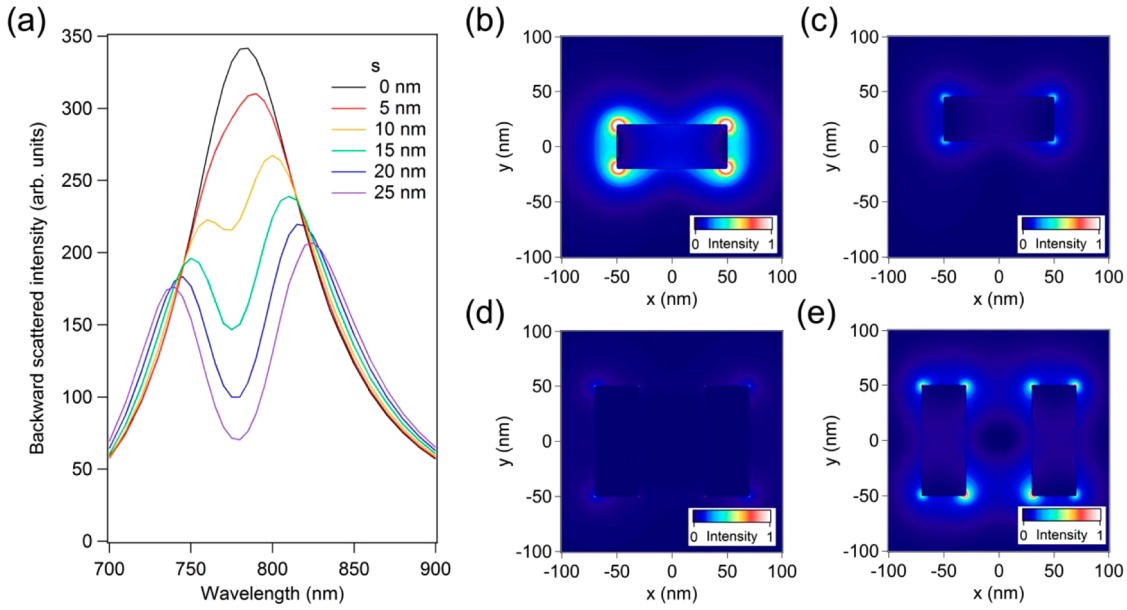

Figure 2. (a) Backward scattered intensity as a function of the wavelength computed for values of the parameter *s* ranging between 0 and 25 nm. Normalized near-field intensity maps close to (b,c) the dipolar nanorod antenna and to (d,e) the two parallel nanorods evaluated for an incident wavelength λ = 780 nm for (b,d) *s* = 0 and (c,e) *s* = 25 nm. The same colorscale is used for the four maps.

allowing designing efficient nonlinear plasmonic nanorulers.

Let us now consider the SH optical response of a gold nanodolmen. It is well-known that SHG is forbidden in the bulk of centrosymmetric media within the electric dipole approximation.[67] Nevertheless, this symmetry is broken at the interface between two centrosymmetric media and SHG arises from metallic nanostructure surfaces.[67] Surface integral equations methods only require the discretization of the surfaces of the metal nanostructures, exactly where the SHG sources are located, and are therefore extremely well suited for accurate SHG computations, as recently demonstrated by Mäkitalo et al.[68] The numerical method used for SHG computations is described in the Methods section. Figure 3 shows the SH near-field intensity close to the dipolar nanorod antenna and to the two parallel nanorods evaluated for an incident (fundamental) wavelength λ= 780 nm for the symmetric case (*s* = 0) and a nonsymmetric case (*s* = 25 nm). In the symmetric case, the SH near-field intensity is localized close to the top nanobar. Indeed, the SH sources, *i.e.*, the nonlinear polarization sheets standing at the metal-dielectric interfaces, are proportional to the squared normal component of the local fundamental electric field evaluated just below the metallic surface (see Methods for details).[69] Since the fundamental wave is localized close to the top nanorod, this is also the case for the SH wave, and the SH intensity observed close to the two parallel nanoparticles is weak. As previously discussed, the quadrupolar mode supported by the two parallel nanorods is excited if the symmetry is broken.[31,33,36] As a

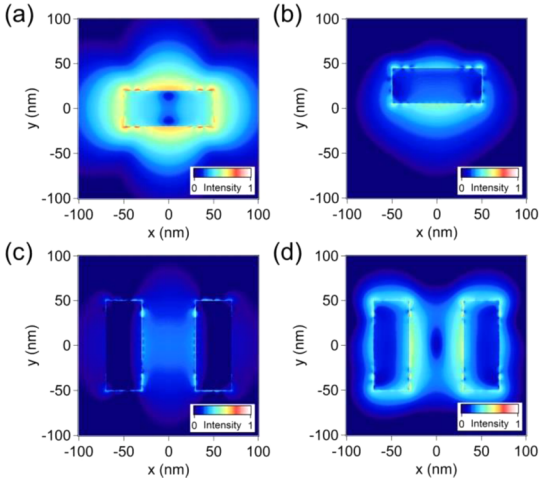

Figure 3. SH near-field intensity maps (shown in a logarithmic scale) close to (a,b) the dipolar nanorod antenna and to (c,d) the two parallel nanorods evaluated for an incident wavelength λ= 780 nm for (a,c) *s* = 0 and (b,d) *s* = 25 nm. The same colorscale is used for the four maps.

consequence, the strength of the SH sources standing at the surface of the two parallel rods increases resulting in an increase of the SH intensity at their vicinity (see Figure 4(d)). Note that the intensity enhancement related to the quadrupolar mode depends on the symmetry parameter *s* and reaches a maximum value in the intermediate coupling regime.[33] These results indicate that the nonlinear sources distribution on plasmonic nanostructures can be controlled using a Fano resonance at the fundamental wavelength. In the following, the influence on the SH far-field radiation will be investigated in detail with the aim of designing sensitive nonlinear remote sensors.

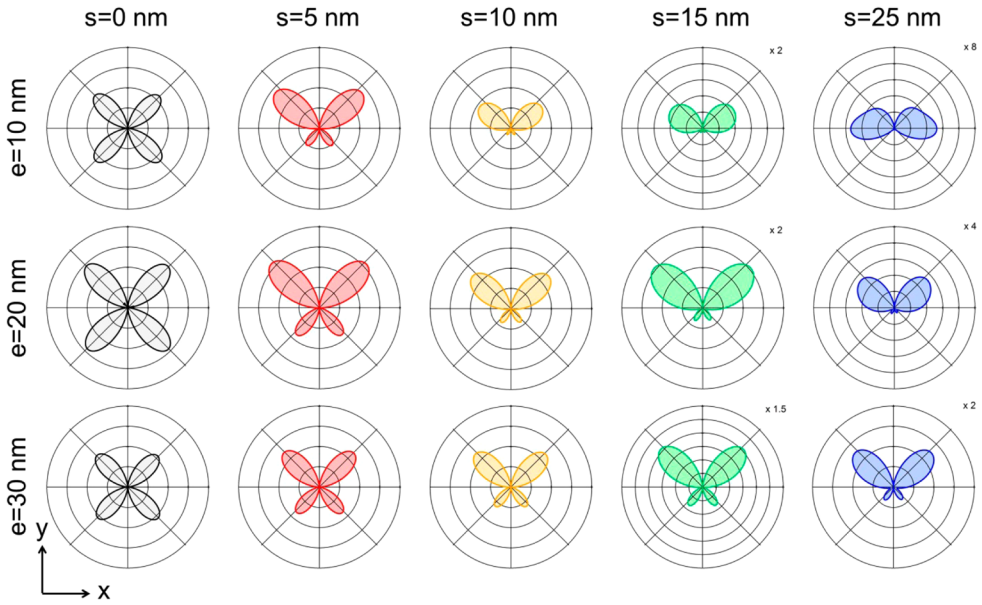

Figure 4. Normalized SH intensity scattered in the vertical (*O*, *x*, *y*) plane as a function of the scattering angle considering the SH scattered wave polarized into the vertical plane. The geometrical parameter *e* = 10 nm (first row), 20 nm (second row), and 30 nm (third row), and the parameter *s* = 0 (black curves), 5 nm (red curves), 10 nm (orange curves), 15 nm (green curves), and 25 nm (bleu curves). The fundamental wavelength is 780 nm. The outer circle corresponds to same intensity for each polar-plots of a given row. Some plots have been multiplied for clarity.

Far-field properties of nonlinear optical processes are key to the design of remote sensing applications in the nonlinear regime. Figure 4 shows for different values of the parameters *s* and *e* the normalized SH intensity scattered in the vertical (*O*, *x*, *y*) plane as a function of the scattering angle, considering the SH scattered wave polarized into the vertical plane. The SH emission pattern evolves from a symmetric four-lobes pattern similar to a quadrupolar emission for $s = 0$ to asymmetric emission patterns for $s \neq 0$. Indeed, SHG from metallic nanostructures with centrosymmetric shapes is forbidden in the electric dipole approximation explaining why high multipolar modes are involved in the nonlinear optical response.[44,45,70] In order to confirm this assumption, the SHG from a single gold nanorod was computed, and a nondipolar response was clearly observed (see Supporting Information, Figure S1). In the case of the symmetric gold nanodolmen ($s = 0$), SH field is generated by the top nanorod, and a SH emission pattern similar to that of a single rod is then expected. For asymmetric nanodolmens, the total SH emission pattern observed in a specific configuration arises from the interference between the SH emissions from the top bar and from the two parallel ones, and their relative weights in the overall signal is controlled by the Fano resonance occurring at the fundamental wavelength. For a given value of the symmetry parameter ($s \neq 0$), the asymmetry of the SH emission pattern increases as the distance between the top rod and the two parallel rods decreases, *i.e.*, as the coupling between the dipolar and quadrupolar modes at the fundamental wavelength increases. The same effect on the SH emission pattern is observed if the parameter *e* is kept constant and the symmetry parameter *s* increases, which also results in an increase of the mode coupling. Note that the mode coupling modifies the directivity of the nonlinear emission as observed in the linear regime for Yagi–Uda nanoantennas.[71,72] These results clearly demonstrate that the SH far-field distribution depends on the two parameters *e* and *s* giving a hint that efficient 3-dimensionnal nonlinear plasmonic nanorulers can be designed.

In order to quantitatively compare different nanodolmen configurations and their emission patterns, an asymmetry parameter *A* is introduced as

$$A = \frac{I_1 - I_2}{I_1} \qquad (1)$$

where I_1 and I_2 are the maximal SH intensity scattered in the upper ($y > 0$) and lower ($y < 0$) parts of the polar-plot, respectively. The asymmetry parameter *A* is reported as a function of the symmetry parameter *s* for different values of the distance *e* between the top nanorod and two parallel nanoparticles. The asymmetry parameter *A* evolves from 0 for symmetric emission pattern where the four-lobes are observed for $s = 0$ to almost 100% for the highest values of the symmetry parameter *s*. The asymmetry parameter *A* dramatically depends on the distance *e*, emphasizing the role played in the nonlinear response by the coupling between the dipolar and the quadrupolar modes at the fundamental wavelength. Figure 6 shows the SH far-field distribution computed considering an incident wavelength longer (λ = 860 nm) and shorter (λ = 700 nm) than the Fano dip wavelength. The obtained

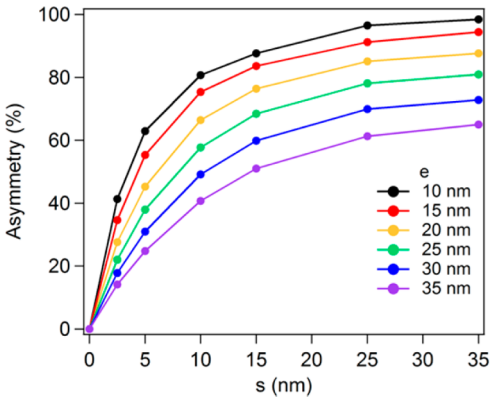

Figure 5. Asymmetry parameter (as defined by eq 1) as a function of the parameter *s* evaluated for different values of the parameter *e* increasing from 10 nm (black curve) to 35 nm (purple curve). The fundamental wavelength is 780 nm.

value of the asymmetry parameter *A* for a given nanodolmen configuration is always lower than the one obtained for an incident wavelength corresponding to Fano dip. This observation confirms the impressive influence of the modes coupling at the fundamental wavelength on the SH response and the active role of the Fano resonance in the designed nonlinear plasmonic ruler.[61] Furthermore, for all values of the distance *e*, the variation of the asymmetry parameter *A* is stronger for small values of the symmetry parameter *s*, *i.e.*, small symmetry breaking. Indeed, it was reported that the properties of the mode are extremely sensitive to small geometric perturbations in the weak coupling regime.[33,36] Figure 5 indicates that ultrasensitive measurement of the top nanorod displacement (resolution: ~1 nm) can be achieved recording the variation of the asymmetry parameter *A*. Note that the predicted resolution can be modified by the presence of defects in fabricated nanostructures (additional simulations performed considering a realistic gold nanodolmen are shown in the Supporting Information (Figure S2) and indicate that even in such a realistic geometry the relative position of the different parts in the structure can be retrieved with a nonlinear readout).[51] Furthermore, the resolution is predicted to decrease as the distance *e* increases. Nevertheless, the coupling strength depends on both the symmetry parameter *s* and the distance *e*, and identical values of the asymmetry parameter *A* could be obtained for different parameter sets (*e*, *s*). As a consequence, the position of the top bar cannot be accurately determined in 3-dimensions recording the asymmetry parameters *A* only. In the following, we will show that considering the SH emission in another scattering plane overcomes this limitation.

In order to demonstrate that the gold nanodolmens discussed in this work can be used as 3-dimensional nonlinear plasmonic rulers, the normalized SH intensity scattered in the horizontal (*O*, *x*, *z*) plane has been

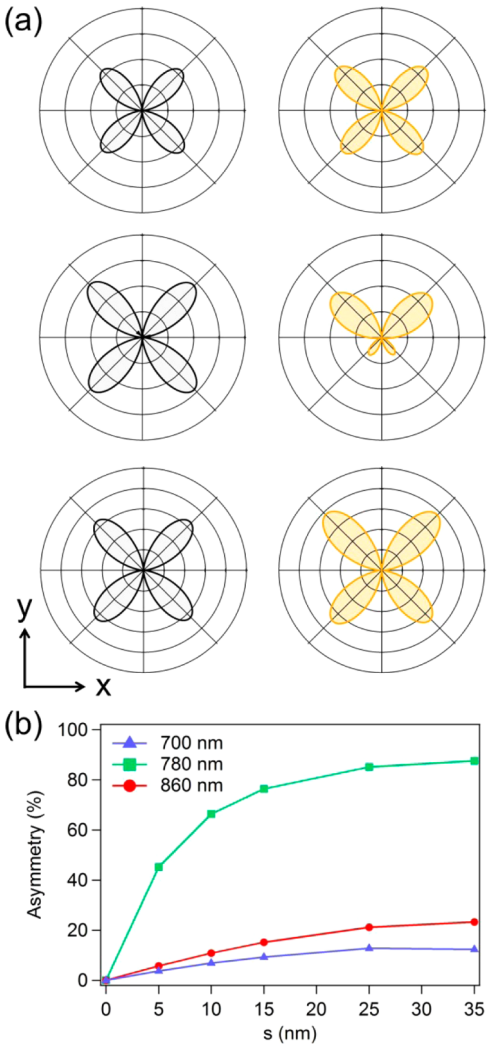

Figure 6. (a) Normalized SH intensity scattered in the vertical (*O*, *x*, *y*) plane as a function of the scattering angle considering the SH scattered wave polarized into the vertical plane. The geometrical parameter is *e* = 20 nm, and the parameter *s* equals 0 (black curves, left side panels) and 10 nm (orange curves, right side panels). The fundamental wavelength is 700 nm (first row), 780 nm (second row), 860 nm (third row). (b) Asymmetry parameter (as defined in eq 1) as a function of the parameter *s* evaluated for an incident wavelength λ = 700 nm (blue triangles), 780 nm (green squares), and 860 nm (red circles).

computed as a function of the scattering angle for different couples (*e*, *s*) corresponding to an asymmetry *A* of ~60% (see Figure 7). The emission patterns observed in this plane are different despite similar values of the asymmetry parameter *A*. These results demonstrate that the position of the top bar can be accurately determined recording the SH intensity scattered into two specific planes. Let us now compare this 3-dimensional nonlinear plasmonic ruler with the linear one previously reported in the literature.[39] The linear 3-dimensional plasmonic ruler is composed of five gold nanorods (a single rod placed in close proximity to two pairs of parallel nanorods).[39,73] One nanorod pair is longer, modifying the spectral position of

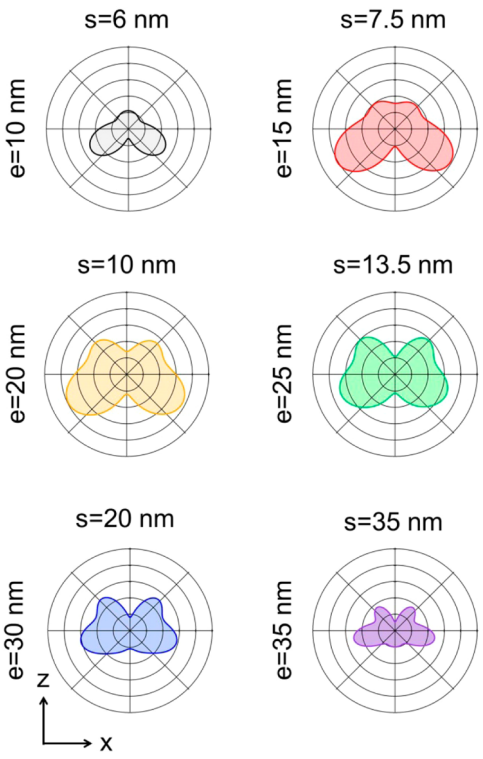

Figure 7. Normalized SH intensity scattered in the horizontal (*O*, *x*, *z*) plane as a function of the scattering direction evaluated for different couples (*e*, *s*) corresponding to an asymmetry of ~60% (see Figure 5): (10 nm, 6 nm) (black curve), (15 nm, 7.5 nm) (red curve), (20 nm, 10 nm) (orange curve), (25 nm, 13.5 nm) (green curve), (30 nm, 20 nm) (blue curve), and (35 nm, 35 nm) (purple curve). The outer circle corresponds to the same intensity for all the polar plots.

the supported quadrupolar mode. A modification of the central nanorod position results in a change in the coupling between the dipolar and the quadrupolar modes and then in the recorded transmittance.[39,73] In the case of SHG from asymmetric nanodolmens, the scattered wave takes origin from the top bar and the two parallel nanorods leading to interferences in the far-field, and the relative weight of the nonlinear sources is controlled using the Fano resonance occurring at the fundamental wavelength. The results presented in this article demonstrate that the accurate determination of the top nanorod position can be realized using the coupling with only one quadrupolar mode if SHG is used instead of the linear optic. This higher sensitivity to the configuration of plasmonic systems is explained by the symmetry properties of SHG. Indeed, SHG is extremely sensitive to minute variation from symmetric configuration.[51] For comparison, the relative linear intensity scattered in the vertical (*O*, *x*, *y*) plane and in the horizontal (*O*, *x*, *z*) plane as a function of the scattering angle is shown in the Supporting Information (Figure S3). As an example, it is observed that the lobes intensity varies by less than 3% in the linear regime (see Figure S3(a), Supporting Information), while the value obtained for SHG is 45% (see Figure S3(c), Supporting Information) for $s = 5$ nm and $e = 20$ nm. Contrary to SH far-field distribution, the asymmetry of the dolmen nanostructures is clearly revealed in the linear scattered field distribution only for the highest values of the symmetry parameter ($s > 15$ nm for $e = 20$ nm) emphasizing the benefit of using SHG for the readout of plasmonic nanorulers. In order to demonstrate that the complete structure configuration can be determined using SHG, additional computations considering rotation of the top nanorod are shown in Figures S4 and S5 (Supporting Information). These calculations indicate that a rotation as small as 10° leads to an asymmetry of 10%, which is clearly observable.

CONCLUSIONS

In summary, the SHG from gold nanodolmens has been numerically investigated using a surface integral equations method. The role played by the Fano resonance arising from the coupling between the dipolar and quadrupolar modes at the fundamental wavelength has been discussed in detail. In particular, the influence of the near-field intensity distribution over the nanodolmen on the nonlinear response has been emphasized demonstrating that the SH far-field distribution is dramatically modified when the quadrupolar mode is resonantly excited. Interestingly, a displacement of the top nanorod is clearly revealed in the SH far-field distribution, and its position can be accurately determined in 3-dimensions, while this cannot be achieved using linear optics. These results show that SHG allows an accurate determination of the plasmonic nanostructure configurations and that SHG is a promising alternative to linear optic for optical sensing at the nanoscale. This work paves the way for the design of nonlinear plasmonic rulers with less complicated geometry than plasmonic rulers working in the linear regime. Furthermore, nonlinear plasmonic rulers are particularly promising for biomedical and chemical applications for which compact nanorulers are expected to be more efficient.

METHODS

The linear optical responses have been calculated using a surface integral formulation. A plane wave polarized along the *x*-axis and propagating along the *z*-axis is always considered. All the nanostructures are considered in water ($n = 1.33$), and the dielectric constants for gold are taken from experimental data at both the fundamental and second harmonic wavelengths.[74] For the SHG computations, the linear surface currents, which are expanded on Rao–Wilton–Glisson (RWG) basis functions,[64,68] are used for the evaluation of the fundamental electric fields just below the gold surfaces and then used for the calculation of the surface SH polarization. For the sake of simplicity, only the component $\chi_{surf,nnn}$ of the surface tensor, where *n* denotes the component normal to the surface, is considered. Recent

experimental results show that this term dominates the surface response of metallic nanoparticles.[75] Note that other contributions to the SH signal, namely, the component $\chi_{surf,ttn}$ of the surface tensor (where *t* denotes the component tangential to the surface) and bulk contribution, are theoretically allowed, but these terms contribute only weakly to the total SH wave.[75,76] Furthermore, the present work is focused on the nonlinear plasmonic rulers, and the obtained results are valid whatever the nonlinear sources. The SH surface currents are obtained solving the SIE formulation taking into account the nonlinear polarization and enforcing the boundary conditions at the nanostructure surfaces.[77] As the linear surface currents, the SH surface currents are expanded on RWG basis functions. The expanding coefficients are found applying the method of moments with Galerkin's testing.[64,68] A Poggio–Miller–Chang–Harrington–Wu formulation is used to ensure accurate solutions even at resonant conditions.[64,68] The SH electric field is then deduced from the SH surface currents using a two-term subtraction method for the evaluation of the Green's functions.[64]

Conflict of Interest: The authors declare no competing financial interest.

Acknowledgment. It is a pleasure to acknowledge T. V. Raziman for his help with the simulation of realistic nanodolmens. Funding from the Swiss National Science Foundation (SNSF, Project 200021_132694) is gratefully acknowledged.

Supporting Information Available: Computations of SHG performed for a single nanorod, a realistic nonlinear plasmonic nanoruler, and a rotation of the top nanorod are shown. A direct comparison with the linear response of the gold nanodolmens is also shown. This material is available free of charge *via* the Internet at http://pubs.acs.org.

REFERENCES AND NOTES

1. Barnes, W. L.; Dereux, A.; Ebbesen, T. W. Surface Plasmon Subwavelength Optics. *Nature* **2003**, *424*, 824–830.
2. Maier, S. A. In *Plasmonics: Fundamentals and Applications*; Springer: New York, 2007.
3. Schuller, J. A.; Barnard, E. S.; Cai, W.; Chul Jun, Y.; White, J. S.; Brongersma, M. L. Plasmonics for Extreme Light Concentration and Manipulation. *Nat. Mater.* **2010**, *9*, 193–204.
4. Martin, O. J. F.; Girard, C.; Dereux, A. Generalized Field Propagator for Electromagnetic Scattering and Light Confinement. *Phys. Rev. Lett.* **1995**, *74*, 526–529.
5. Prodan, E.; Radloff, C.; Halas, N. J.; Nordlander, P. A Hybridization Model for the Plasmon Response of Complex Nanostructures. *Science* **2003**, *302*, 419–422.
6. Halas, N. J.; Lal, S.; Chanq, W.-S.; Link, S.; Nordlander, P. Plasmons in Strongly Coupled Metallic Nanostructures. *Chem. Rev.* **2011**, *111*, 3913–3961.
7. Nordlander, P.; Oubre, C.; Prodan, E.; Li, K.; Stockman, M. I. Plasmon Hybridization in Nanoparticle Dimers. *Nano Lett.* **2004**, *4*, 899–903.
8. Jain, P. K.; Huang, W.; El-Sayed, M. A. On the Universal Scaling Behavior of the Distance Decay of Plasmon Coupling in Metal Nanoparticle Pairs: A Plasmon Ruler Equation. *Nano Lett.* **2007**, *7*, 2080–2088.
9. Sonnichsen, C.; Reinhard, B. M.; Liphardt, J.; Alivisatos, A. P. A Molecular Ruler Based on Plasmon Coupling of Single Gold and Silver Nanoparticles. *Nat. Biotechnol.* **2005**, *23*, 741–745.
10. Wang, J.; Boriskina, S. V.; Wang, H.; Reinhard, B. M. Illuminating Epidermal Growth Factor Receptor Densities on Filopodia through Plasmon Coupling. *ACS Nano* **2011**, *5*, 6619–6628.
11. Yang, L.; Wang, H.; Yan, B.; Reinhard, B. M. Calibration of Silver Plasmon Rulers in 1–25 nm Separation Range: Experimental Indications of Distinct Plasmon Coupling Regimes. *J. Phys. Chem. C* **2010**, *114*, 4901–4908.
12. Anker, J. N.; Hall, W. P.; Lyandres, O.; Shah, N. C.; Zhao, J.; Van Duyne, R. P. Biosensing with Plasmonic Nanosensors. *Nat. Mater.* **2008**, *7*, 442–452.
13. Luk'yanchuck, B.; Zheludev, N. I.; Maier, S. A.; Halas, N. J.; Nordlander, P.; Giessen, H.; Chong, C. T. The Fano Resonance in Plasmonic Nanostructures and Metamaterials. *Nat. Mater.* **2010**, *9*, 707–715.
14. Miroshnichenko, A. E.; Flach, S.; Kivshar, Y. S. Fano Resonances in Nanoscale Structures. *Rev. Mod. Phys.* **2010**, *82*, 2257–2298.
15. Hao, F.; Nordlander, P.; Sonnefraud, Y.; Van Dorpe, P.; Maier, S. A. Tunability of Subradiant Dipolar and Fano-Type Plasmon Resonances in Metallic Ring/Disk Cavities: Implications for Nanoscale Optical Sensing. *ACS Nano* **2009**, *3*, 643–652.
16. Fu, Y. H.; Zhang, J. B.; Yu, Y. F.; Luk'yanchuk, B. Generating and Manipulating Higher Order Fano Resonances in Dual-Disk Ring Plasmonic Nanostructures. *ACS Nano* **2012**, *6*, 5130–5137.
17. Cetin, A. E.; Altug, H. Fano Resonant Ring/Disk Nanocavities on Conducting Substrates for Advanced Biosensing. *ACS Nano* **2012**, *6*, 9989–9995.
18. Wu, C.; Khanikaev, A. B.; Adato, R.; Arju, N.; Yanik, A. A.; Altug, H.; Shvets, G. Fano-Resonant Asymmetric Metamaterials for Ultrasensitive Spectroscopy and Identification of Molecular Monolayers. *Nat. Mater.* **2012**, *11*, 69–75.
19. Verellen, N.; Sonnefraud, Y.; Sobhani, H.; Hao, F.; Moshchalkov, V. V.; Van Dorpe, P.; Nordlander, P.; Maier, S. A. Fano Resonances in Individual Coherent Plasmonic Nanocavities. *Nano Lett.* **2009**, *9*, 1663–1667.
20. Liu, N.; Weiss, T.; Mesch, M.; Langguth, L.; Eigenthaler, U.; Hirscher, M.; Soennichsen, C.; Giessen, H. Planar Metamaterial Analogue of Electromagnetically Induced Transparency for Plasmonic Sensing. *Nano Lett.* **2010**, *10*, 1103–1107.
21. Fan, J. A.; Wu, C.; Bao, K.; Bao, J.; Bardhan, R.; Halas, N. J.; Manoharan, V. N.; Nordlander, P.; Shvets, G.; Capasso, F. Self-Assembled Plasmonic Nanoparticle Clusters. *Science* **2010**, *328*, 1135–1138.
22. Lassiter, J. B.; Sobhani, H.; Fan, J. A.; Kundu, J.; Capasso, F.; Nordlander, P.; Halas, N. J. Fano Resonances in Plasmonic Nanoclusters: Geometrical and Chemical Tunability. *Nano Lett.* **2010**, *10*, 3184–3189.
23. Hentschel, M.; Saliba, M.; Vogelgesang, R.; Giessen, H.; Alivisatos, A. P.; Liu, N. Transition from Isolated to Collective Modes in Plasmonic Oligomers. *Nano Lett.* **2010**, *10*, 2721–2726.
24. Hentschel, M.; Dregely, D.; Vogelgesang, R.; Giessen, H.; Liu, N. Plasmonic Oligomers: The Role of Individual Particles in Collective Behavior. *ACS Nano* **2011**, *5*, 2042–2050.
25. Gallinet, B.; Martin, O. J. F. *Ab-Initio* Theory of Fano Resonances in Plasmonic Nanostructures and Metamaterials. *Phys. Rev. B: Condens. Matter Mater. Phys.* **2011**, *83*, 235427.
26. Gallinet, B.; Martin, O. J. F. Influence of Electromagnetic Interactions on the Line Shape of Plasmonic Fano Resonances. *ACS Nano* **2011**, *5*, 8999–9008.
27. Giannini, V.; Francescato, Y.; Amrania, H.; Phillips, C. C.; Maier, S. A. Fano Resonances in Nanoscale Plasmonic Systems: A Parameter-Free Modeling Approach. *Nano Lett.* **2011**, *11*, 2835–2840.
28. Rahmani, M.; Lei, D. Y.; Giannini, V.; Lukiyanchuk, B.; Ranjbar, M.; Liew, T. Y. F.; Hong, M.; Maier, S. A. Subgroup Decomposition of Plasmonic Resonances in Hybrid Oligomers: Modeling the Resonance Lineshape. *Nano Lett.* **2012**, *6*, 2101–2106.
29. Lovera, A.; Gallinet, B.; Nordlander, P.; Martin, O. J. F. Mechanisms of Fano Resonances in Coupled Plasmonic Systems. *ACS Nano* **2013**, *7*, 4527–4536.
30. Zhang, S.; Genov, D. A.; Wang, Y.; Liu, M.; Zhang, X. Plasmon-Induced Transparency in Metamaterials. *Phys. Rev. Lett.* **2008**, *101*, 047401.
31. Liu, N.; Langguth, L.; Weiss, T.; Kaestel, J.; Fleischhauer, M.; Pfau, T.; Giessen, H. Plasmonic Analogue of Electromagnetically Induced Transparency at the Drude Damping Limit. *Nat. Mater.* **2009**, *8*, 758–762.
32. Shao, L.; Fang, C.; Chen, H.; Man, Y. C.; Wang, J.; Lin, H.-Q. Distinct Plasmonic Manifestation on Gold Nanorods

Induced by the Spatial Perturbation of Small Gold Nanospheres. *Nano Lett.* **2012**, *12*, 1424–1430.
33. Gallinet, B.; Siegfried, T.; Sigg, H.; Nordlander, P.; Martin, O. Plasmonic Radiance: Probing Structure at the Angstrom Scale with Visible Light. *Nano Lett.* **2013**, *13*, 497–503.
34. Verellen, N.; Van Dorpe, P.; Huang, C.; Lodewijks, K.; Vandenbosch, G. A. E.; Lagae, L.; Moshchalkov, V. V. Plasmon Line Shaping Using Nanocrosses for High Sensitivity Localized Surface Plasmon Resonance Sensing. *Nano Lett.* **2011**, *11*, 391–397.
35. Ye, J.; Wen, F.; Sobhani, H.; Lassiter, J. B.; Van Dorpe, P.; Nordlander, P.; Halas, N. J. Plasmonic Nanoclusters: Near-Field Properties of the Fano Resonance Interrogated with Sers. *Nano Lett.* **2012**, *12*, 1660–1667.
36. Gallinet, B.; Martin, O. J. F. Refractive Index Sensing with Subradiant Modes: A Framework to Reduce Losses in Plasmonic Nanostructures. *ACS Nano* **2013**, 6978–6987.
37. Luk'yanchuk, B. S.; Zheng, Y. W.; Lu, Y. F. Laser Cleaning of Solid Surface: Optical Resonance and Near-Field Effects. *Proc. SPIE* **2000**, *4065*, 576–587.
38. Leveque, G.; Martin, O. J. F. Optical Interactions in a Plasmonic Particle Coupled to a Metallic Film. *Opt. Express* **2006**, *14*, 9971–9981.
39. Liu, N.; Hentschel, M.; Weiss, T.; Alivisatos, A. P.; Giessen, H. Three-Dimensional Plasmon Rulers. *Science* **2011**, *332*, 1407–1410.
40. Kauranen, M.; Zayats, A. V. Nonlinear Plasmonics. *Nat. Photonics* **2012**, *6*, 737–748.
41. Bouhelier, A.; Beversluis, M.; Hartschuch, A.; Novotny, L. Near-Field Second-Harmonic Generation Induced by Local Field Enhancement. *Phys. Rev. Lett.* **2003**, *90*, 013903.
42. Jin, R. C.; Jureller, J. E.; Kim, H. Y.; Scherer, N. F. Correlating Second Harmonic Optical Responses of Single Ag Nanoparticles with Morphology. *J. Am. Chem. Soc.* **2005**, *127*, 12482–12483.
43. Valev, V. K.; Smisdom, N.; Silhanek, A. V.; De Clercq, B.; Gillijns, W.; Ameloot, M.; Moshchalkov, V. V.; Verbiest, T. Plasmonic Ratchet Wheels: Switching Circular Dichroism by Arranging Chiral Nanostructures. *Nano Lett.* **2009**, *9*, 3945–3948.
44. Butet, J.; Duboisset, J.; Bachelier, G.; Russier-Antoine, I.; Benichou, E.; Jonin, C.; Brevet, P.-F. Optical Second Harmonic Generation of Single Metallic Nanoparticles Embedded in a Homogeneous Medium. *Nano Lett.* **2010**, *10*, 1717–1721.
45. Butet, J.; Bachelier, G.; Russier-Antoine, I.; Jonin, C.; Benichou, E.; Brevet, P.-F. Interference between Selected Dipoles and Octupoles in the Optical Second-Harmonic Generation from Spherical Gold Nanoparticles. *Phys. Rev. Lett.* **2010**, *105*, 077401.
46. Zhang, Y.; Grady, N. K.; Ayala-Orozco, C.; Halas, N. J. Three-Dimensional Nanostructures as Highly Efficient Generators of Second Harmonic Light. *Nano Lett.* **2011**, *11*, 5519–5523.
47. Husu, H.; Siikanen, R.; Mäkitalo, J.; Lehtolahti, J.; Laukkanen, J.; Kuittinen, M.; Kauranen, M. Metamaterials with Tailored Nonlinear Optical Response. *Nano Lett.* **2012**, *12*, 673–677.
48. Czaplicki, R.; Husu, H.; Siikanen, R.; Mäkitalo, J.; Kauranen, M. Enhancement of Second-Harmonic Generation from Metal Nanoparticles by Passive Elements. *Phys. Rev. Lett.* **2013**, *110*, 093902.
49. Butet, J.; Russier-Antoine, I.; Jonin, C.; Lascoux, N.; Benichou, E.; Brevet, P.-F. Sensing with Multipolar Second Harmonic Generation from Spherical Metallic Nanoparticles. *Nano Lett.* **2012**, *12*, 1697–1701.
50. Bautista, G.; Huttunen, M. J.; Mäkitalo, J.; Kontio, J. M.; Simonen, J.; Kauranen, M. Second-Harmonic Generation Imaging of Metal Nano-Objects with Cylindrical Vector Beams. *Nano Lett.* **2012**, *12*, 3207–3212.
51. Butet, J.; Thyagarajan, K.; Martin, O. J. F. Ultrasensitive Optical Shape Characterization of Gold Nanoantennas Using Second Harmonic Generation. *Nano Lett.* **2013**, *13*, 1787–1792.
52. Valev, V. K.; Volodin, A.; Silhanek, A. V.; Gillijns, W.; De Clercq, B.; Jeyaram, Y.; Paddubrouskaya, H.; Biris, C. G.; Panoiu, N. C.; Aktsipetrov, O. A.; *et al.* Plasmons Reveal the Direction of Magnetization in Nickel Nanostructures. *ACS Nano* **2011**, *5*, 91–96.
53. Valev, V. K. Characterization of Nanostructured Plasmonic Surfaces with Second Harmonic Generation. *Langmuir* **2012**, *28*, 15454–15471.
54. Shen, H.; Nguyen, N.; Gachet, D.; Maillard, V.; Toury, T.; Brasselet, S. Nanoscale Optical Properties of Metal Nanoparticles Probed by Second Harmonic Generation Microscopy. *Opt. Express* **2013**, *21*, 12318–12326.
55. Anderson, A.; Deryckx, K. S.; Xu, X. G.; Steinmeyer, G.; Raschke, M. B. Few-Femtosecond Plasmon Dephasing of a Single Metallic Nanostructure from Optical Response Function Reconstruction by Interferometric Frequency Resolved Optical Gating. *Nano Lett.* **2010**, *10*, 2519–2524.
56. Berweger, S.; Atkin, J. M.; Xu, X. G.; Olmon, R. L.; Raschke, M. B. Femtosecond Nanofocusing with Full Optical Waveform Control. *Nano Lett.* **2011**, *11*, 4309–4313.
57. Butet, J.; Russier-Antoine, I.; Jonin, C.; Lascoux, N.; Benichou, E.; Martin, O. J. F.; Brevet, P.-F. Universal Scaling of Plasmon Coupling in Metal Nanostructures: Checking the Validity for Higher Plasmonic Modes using Second Harmonic Generation. *Phys. Rev. B: Condens. Matter Mater. Phys.* **2013**, *87*, 235437.
58. Harutyunyan, H.; Volpe, G.; Quidant, R.; Novotny, L. Enhancing the Nonlinear Optical Response Using Multifrequency Gold-Nanowire Antennas. *Phys. Rev. Lett.* **2012**, *108*, 217403.
59. Thyagarajan, K.; Rivier, S.; Lovera, A.; Martin, O. J. F. Enhanced Second-Harmonic Generation from Double Resonant Plasmonic Antennae. *Opt. Express* **2012**, *20*, 12860–12865.
60. Aouani, H.; Navarro-Cia, M.; Rahmani, M.; Sidiropoulos, T. P. H.; Hong, M.; Oulton, R. F.; Maier, S. A. Multiresonant Broadband Optical Antennas As Efficient Tunable Nanosources of Second Harmonic Light. *Nano Lett.* **2012**, *12*, 4997–5002.
61. Thyagarajan, K.; Butet, J.; Martin, O. J. F. Augmenting Second Harmonic Generation Using Fano Resonances in Plasmonic Systems. *Nano Lett.* **2013**, *13*, 1847–1851.
62. Zhang, Y.; Wen, F.; Zhen, Y. R.; Nordlander, P.; Halas, N. J. Coherent Fano Resonances in a Plasmonic Nanocluster Enhance Optical Four-Wave Mixing. *Proc. Natl. Acad. Sci. U. S. A.* **2013**, *110*, 9215–9219.
63. Walsh, G. F.; Dal Negro, L. Enhanced Second Harmonic Generation by Photonic-Plasmonics Fano-Type Coupling in Nanoplasmonic Arrays. *Nano Lett.* **2013**, *13*, 3111–3117.
64. Kern, A. M.; Martin, O. J. F. Surface Integral Formulation for 3D Simulation of Plasmonic and High Permittivity Nanostructures. *J. Opt. Soc. Am. A* **2009**, *26*, 732–740.
65. Kern, A. M.; Martin, O. J. F. Excitation and Reemission of Molecules near Realistic Plasmonic Nanostructures. *Nano Lett.* **2011**, *11*, 482–487.
66. Gallinet, B.; Martin, O. J. F. The Relation Between Near-field and Far-field Properties of Plasmonic Fano Resonances. *Opt. Express* **2011**, *19*, 22167–22175.
67. Boyd, R. W. *Nonlinear Optics*; Academic Press: New York, 1992.
68. Mäkitalo, J.; Suuriniemi, S.; Kauranen, M. Boundary Element Method for Surface Nonlinear Optics of Nanoparticles. *Opt. Express* **2011**, *19*, 23386–23399.
69. Sipe, J. E.; So, C. Y.; Fukui, M.; Stegeman, G. I. Analysis of Second-Harmonic Generation at Metal Surfaces. *Phys. Rev. B: Condens. Matter Mater. Phys.* **1980**, *21*, 4389–4402.
70. Dadap, J. I.; Shan, J.; Eisenthal, K. B.; Heinz, T. F. Second-Harmonic Rayleigh Scattering from a Sphere of Centrosymmetric Material. *Phys. Rev. Lett.* **1999**, *83*, 4045–4048.
71. Pakizeh, T.; Käll, M. Unidirectional Ultracompact Optical Nanoantennas. *Nano Lett.* **2009**, *9*, 2343–2349.
72. Li, J.; Salandrino, A.; Engheta, N. Shaping Light Beams in the Nanometer Scale: A Yagi-Uda Nanoantenna in the Optical Domain. *Phys. Rev. B: Condens. Matter Mater. Phys.* **2007**, *76*, 245403.

73. Davis, T. J.; Hentschel, M.; Liu, N.; Giessen, H. Analytical Model of the Three-Dimensional Plamonic Ruler. *ACS Nano* **2012**, *6*, 1291–1298.
74. Johnson, P. B.; Christy, R. W. Optical Constants of the Noble Metals. *Phys. Rev. B: Solid State* **1972**, *6*, 4370–4379.
75. Bachelier, G.; Butet, J.; Russier-Antoine, I.; Jonin, C.; Benichou, E.; Brevet, P.-F. Origin of Optical Second-Harmonic Generation in Spherical Gold Nanoparticles: Local Surface and Nonlocal Bulk Contributions. *Phys. Rev. B: Condens. Matter Mater. Phys.* **2010**, *82*, 235403.
76. Wang, F. X.; Rodriguez, F. J.; Albers, W. M.; Ahorinta, R.; Sipe, J. E.; Kauranen, M. Surface and Bulk Contributions to the Second-Order Nonlinear Optical Response of a Gold Film. *Phys. Rev. B: Condens. Matter Mater. Phys.* **2009**, *80*, 233402.
77. Heinz, T. F. Second-Order Nonlinear Optical Effects at Surfaces and Interfaces. In *Nonlinear Surface Electromagnetic Phenomena*; Ponath, H.-E., Stegeman, G. I., Eds.; Elsevier: Amsterdam, 1991.